Supplement of Ocean Sci., 22, 2725–2742, 2026
https://doi.org/10.5194/os-22-2725-2026-supplement

Ocean Science
Open Access

Supplement of

The added value of Med-CORDEX coupled high-resolution regional climate models in representing sea surface temperature and marine heatwaves in the Mediterranean Sea

Francesco De Rovere et al.

Correspondence to: Francesco De Rovere (francesco.derovere@cmcc.it)

Table S1. Observational and reanalysis products used in this study.

Product name	Abbreviation	Type	Hor. Res.	Frequency	Period	Description	Reference
Mediterranean Sea High Resolution and Ultra High Resolution SST Analysis	L4-SST	L4 satellite	1/16°	Daily	1982–present	Night-time foundation SST	Pisano et al. (2016); Embury et al. (2024)
Mediterranean Sea High Resolution Diurnal Subskin SST Analysis	SubSkinT	L4 satellite	1/16°	Hourly	2019–present	Sub-skin SST including diurnal cycle	Marullo et al. (2014); Buongiorno Nardelli et al. (2013)
Mediterranean Sea Physics Reanalysis	MEDREA	Ocean reanalysis	1/24°	Daily	1987–2022	Reanalysed SST and ocean state	Escudier et al. (2021)

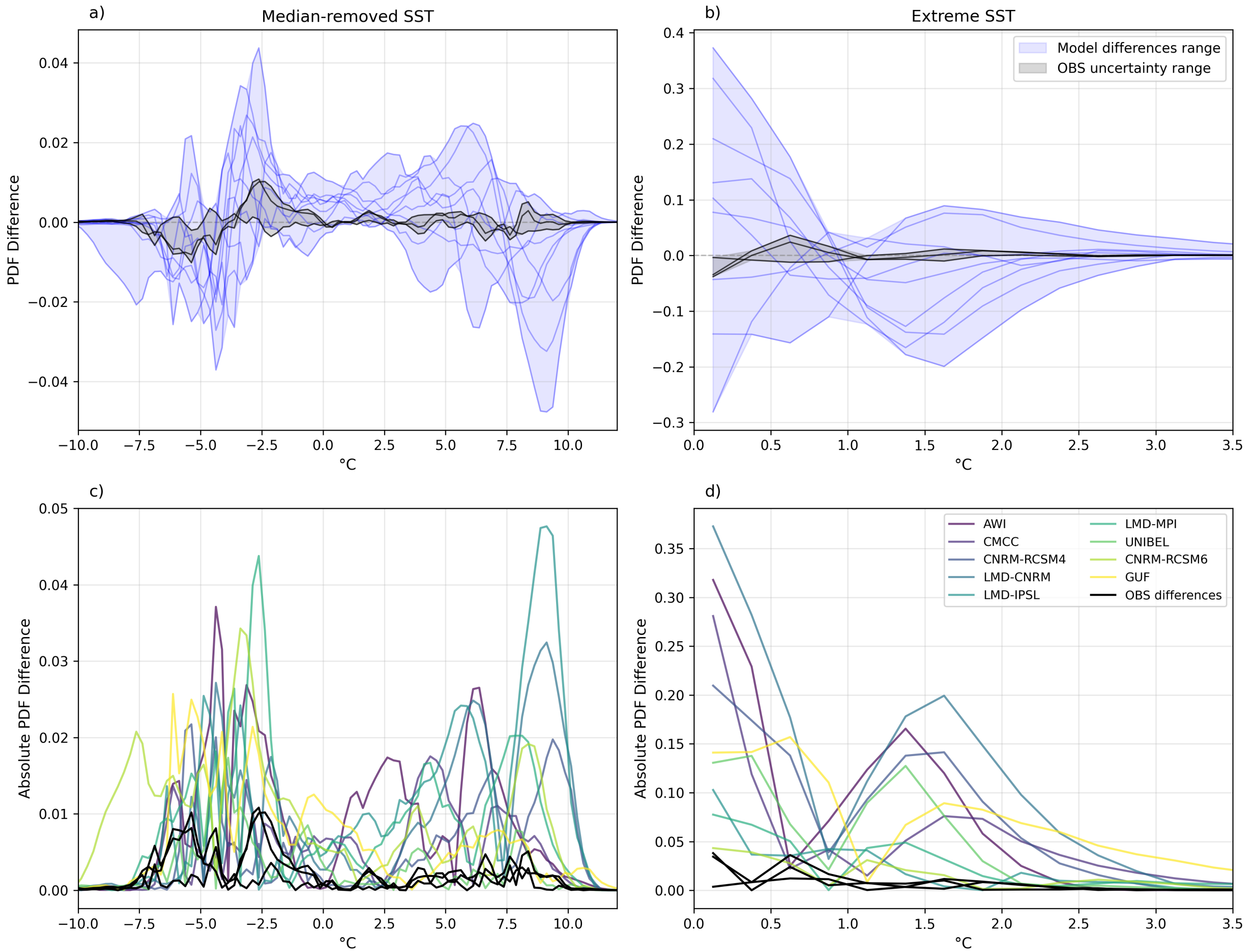

Figure S1. Comparison of PDF differences between RCSM–GCM pairs and among observational products, for median-removed SST (left column) and extreme SST (right column). Top row: PDF differences; bottom row: absolute PDF differences. The data period is from 2019 to 2022.

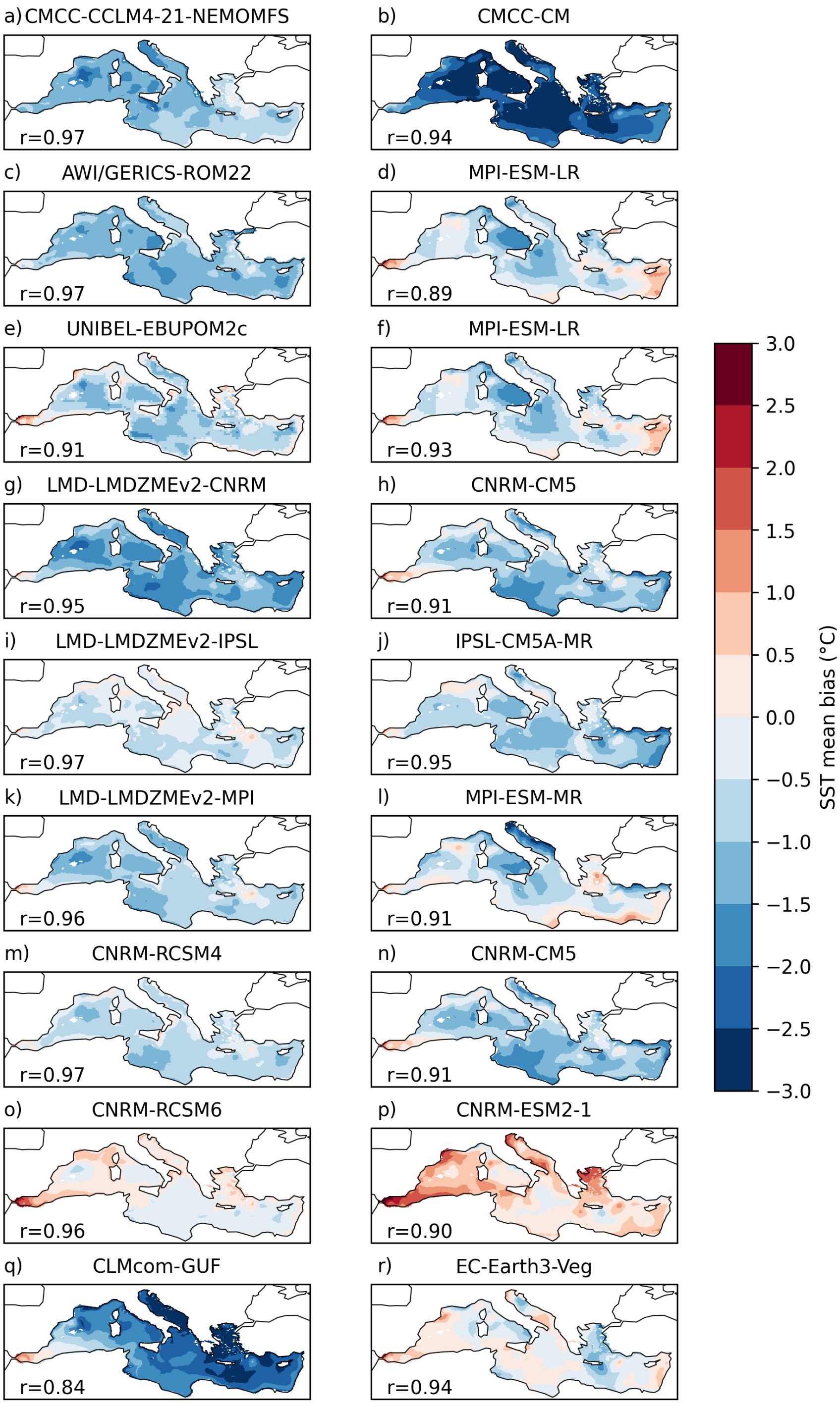

Figure S2. Mean SST biases for the RCSM (left column) and GCM (right column). The pattern correlation of mean SST maps between each model and OBS is shown in each panel.

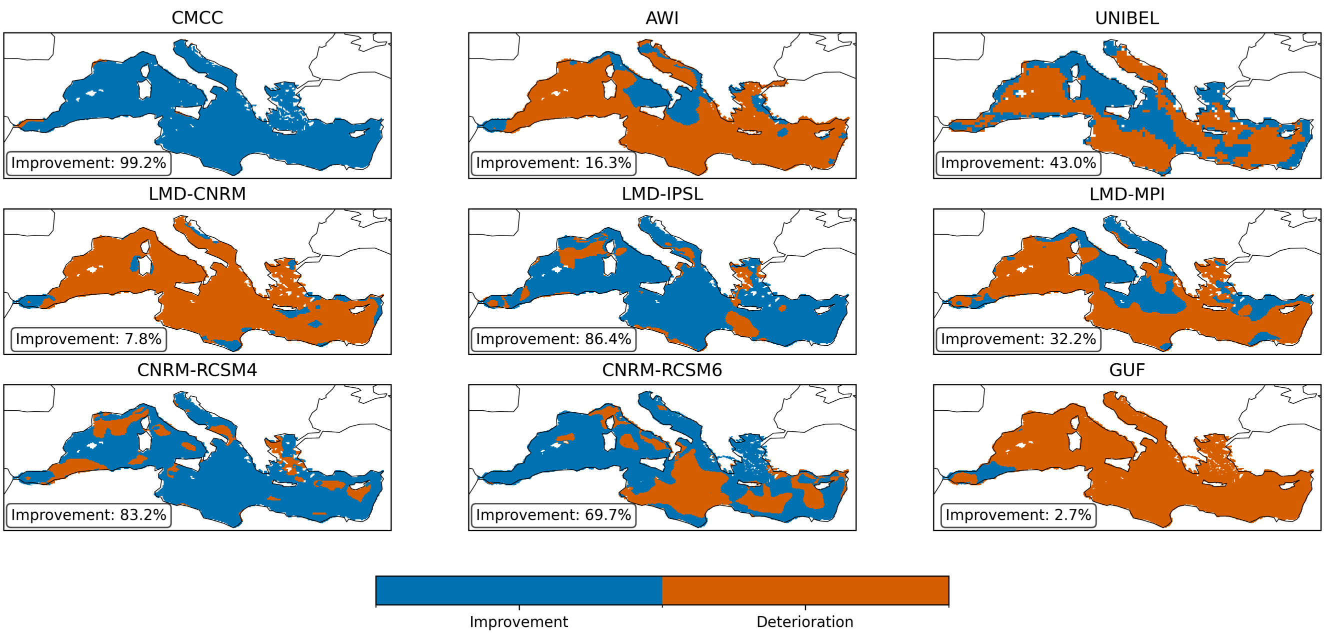

Figure S3. Spatial distribution of mean SST bias improvement for each RCSM. Blue (orange) grid points indicate where the RCSM absolute bias is lower (higher) than that of the driving GCM. The fraction of improved grid points is reported in each panel.

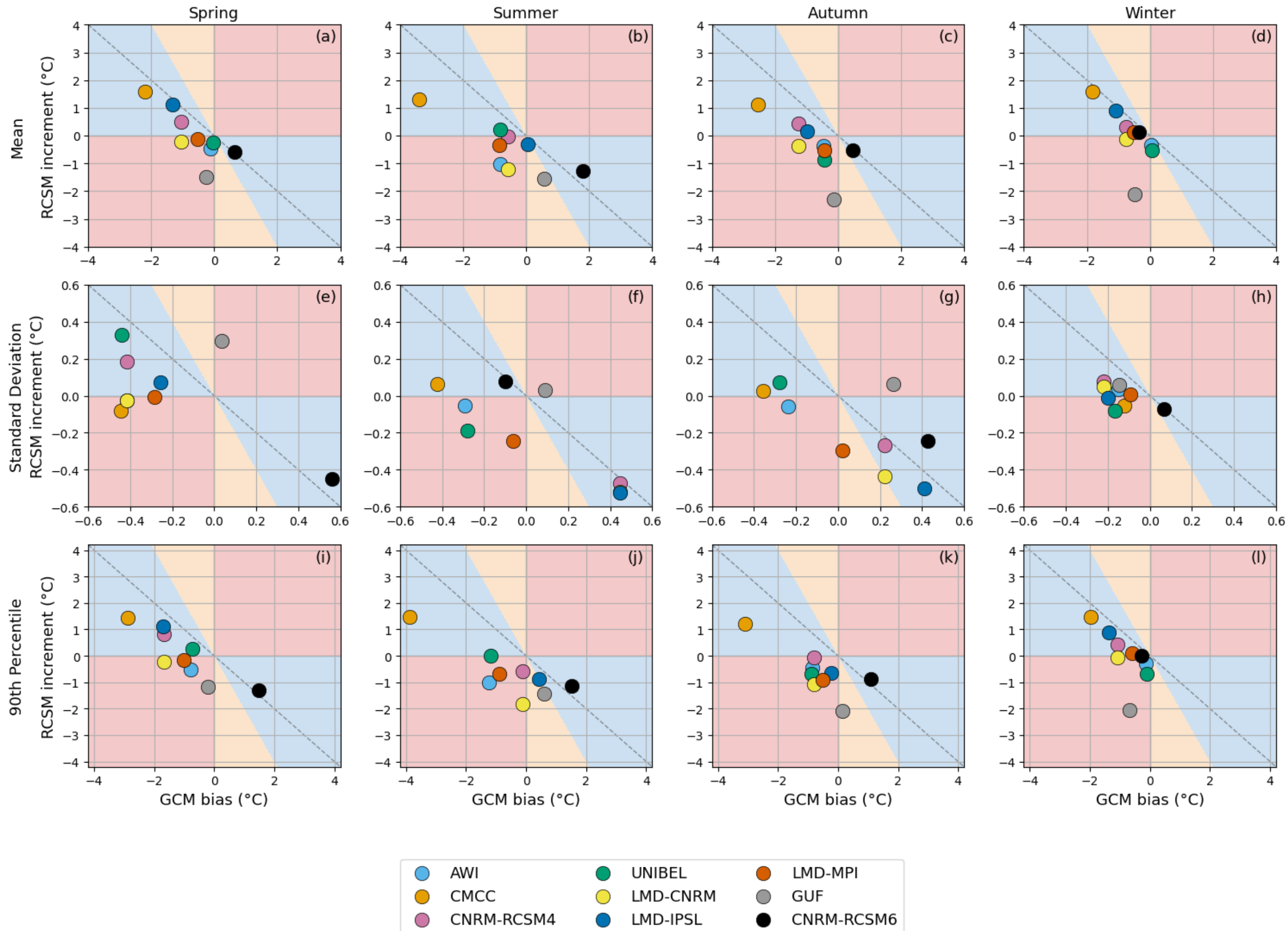

Figure S4. RCSMs increment vs GCM bias, formatted as in Figure 1 of the manuscript for area-averaged SST (a,b,c,d) mean, (e,f,g,h) standard deviation and (i,j,k,l), for (a,e,i) spring, (b,f,j) summer, (c,g,k) autumn and (d,h,l) winter in 1982-2020.

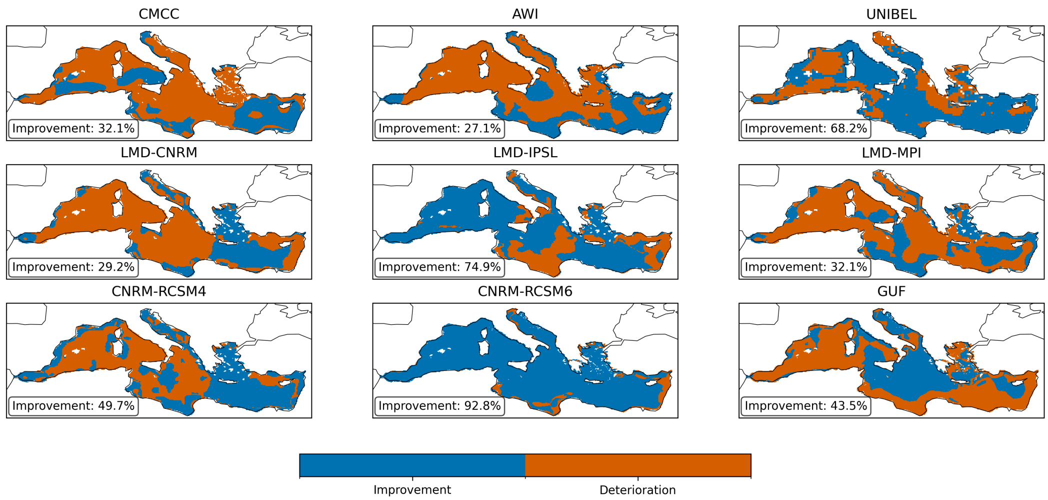

Figure S5. As in Figure S3, but for the standard deviation of SST.

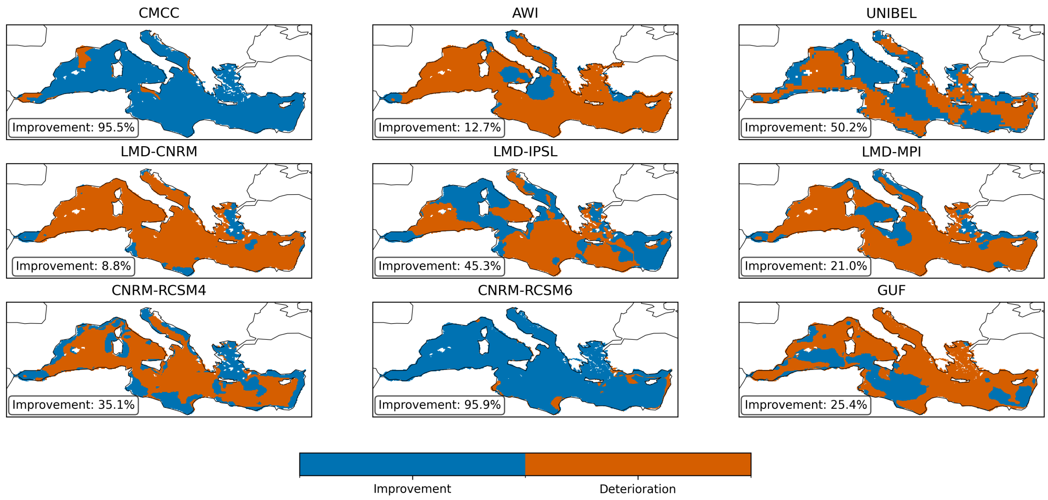

Figure S6. As in Figure S3, but for the SST 90th percentile.

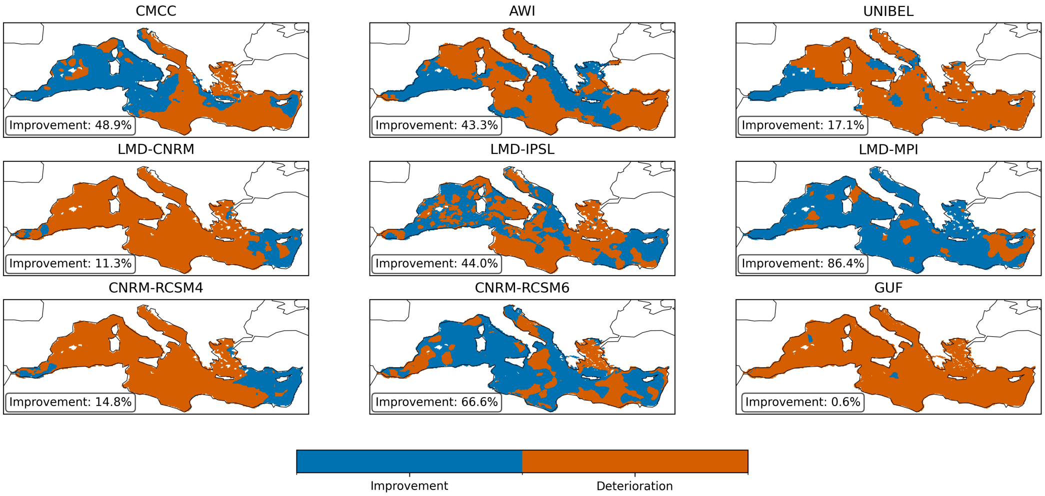

Figure S7. As in Figure S3, but for the SST trend.

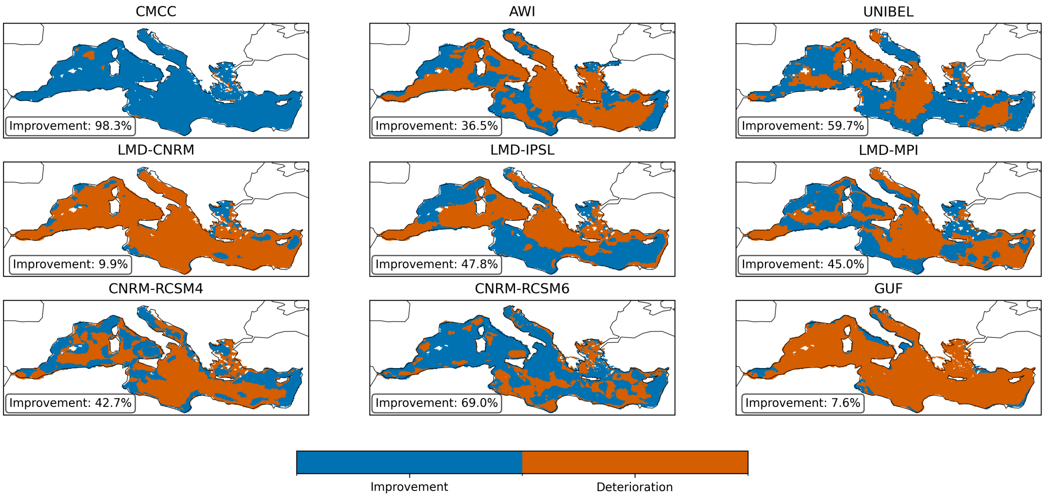

Figure S8. As in Figure S3, but for the standard deviation of SST residuals.

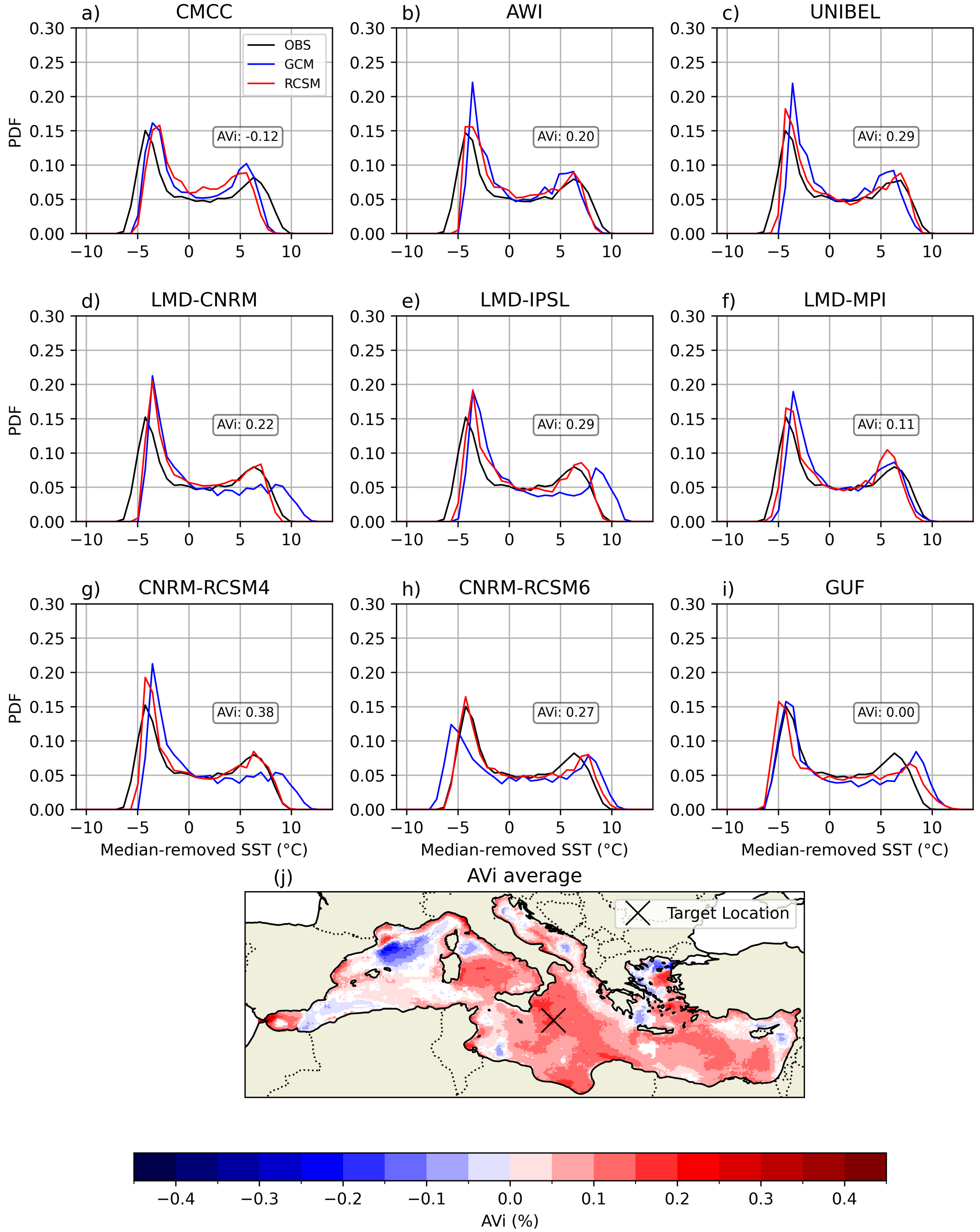

Figure S9. PDFs of median-removed SST at a point in the central Mediterranean (36° N, 17° E) for (a) CMCC, (b) AWI, (c) UNIBEL, (d) LMD-CNRM, (e) LMD-IPSL, (f) LMD-MPI, (g) CNRM-RCSM4, (h) CNRM-RCSM6, and (i) GUF. Lines show observations (black), RCSMs (red), and driving GCMs (blue). Panel j) shows the multi-model AVi mean (as in Figure 2 of the manuscript).

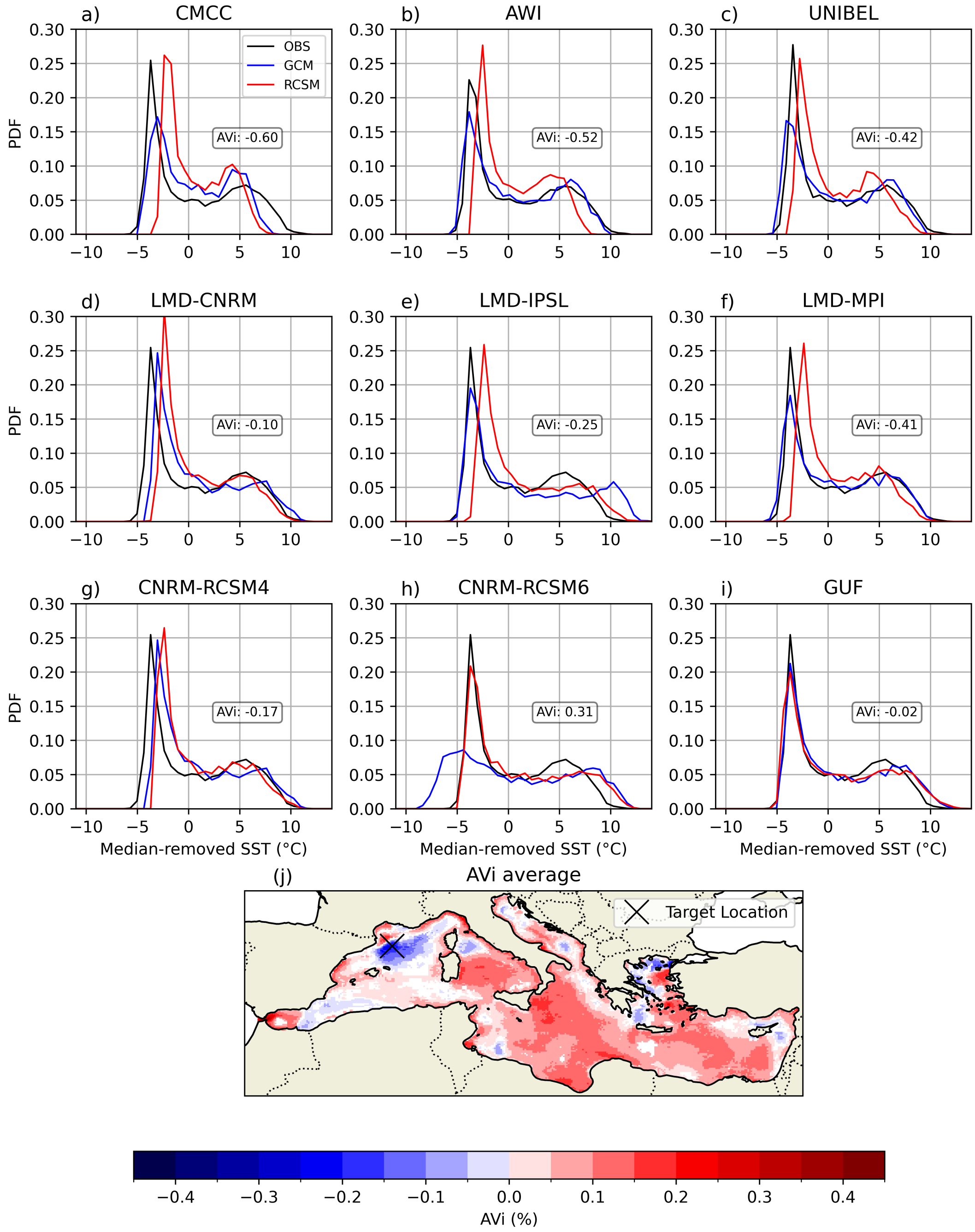

Figure S10. As in Figure S9 but for a point in the Gulf of Lion (41.7° N, 4.5° E).

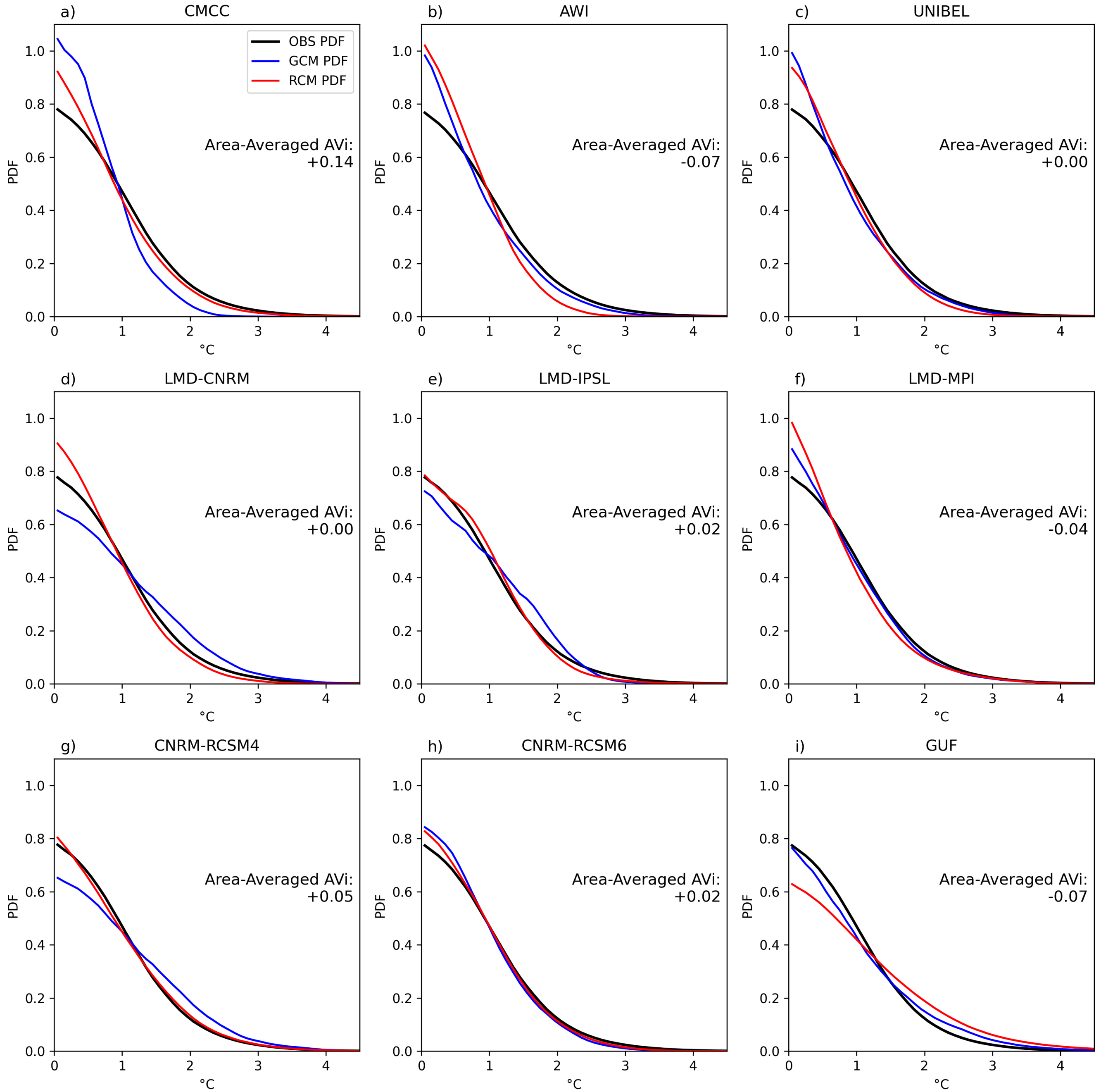

Figure S11. PDFs of upper tail SST (anomalies above the 90th percentile) for (a) CMCC, (b) AWI, (c) UNIBEL, (d) LMD-CNRM, (e) LMD-IPSL, (f) LMD-MPI, (g) CNRM-RCSM4, (h) CNRM-RCSM6, and (i) GUF. Lines show observations (black), RCSMs (red), and driving GCMs (blue). PDFs are computed by aggregating data from all grid points in the Mediterranean basin.

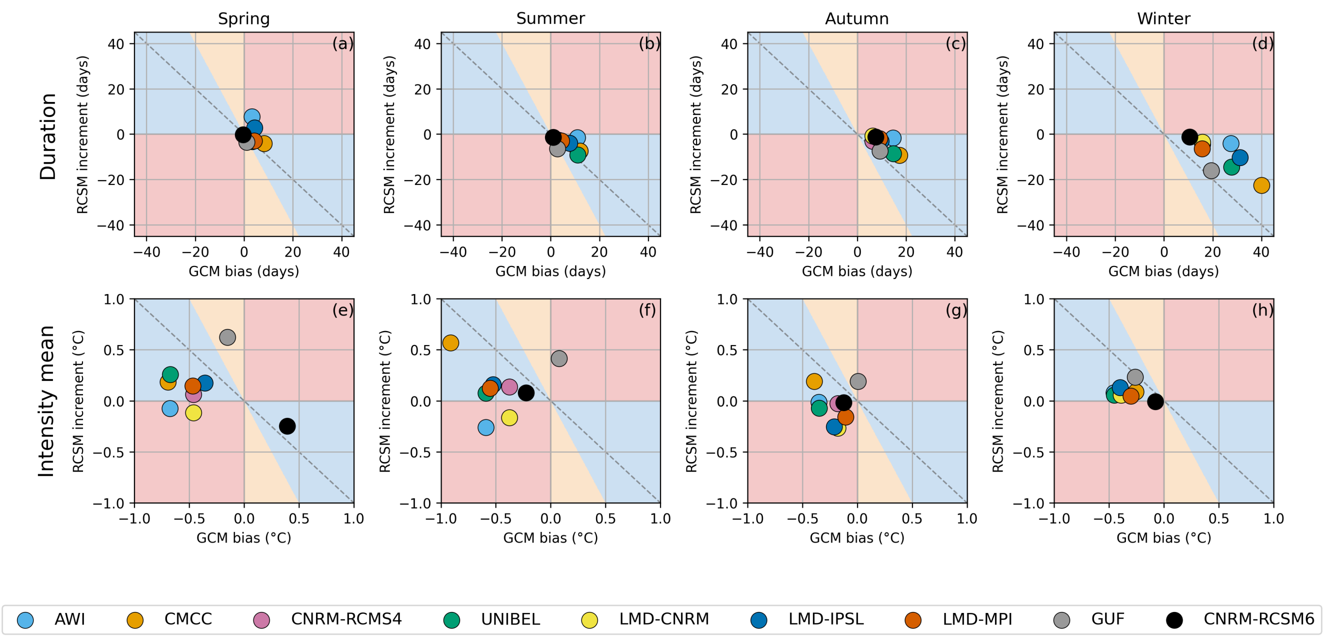

Figure S12. As in Figure S4 but for area-averaged MHW properties, calculated using a fixed baseline in 1982-2011.

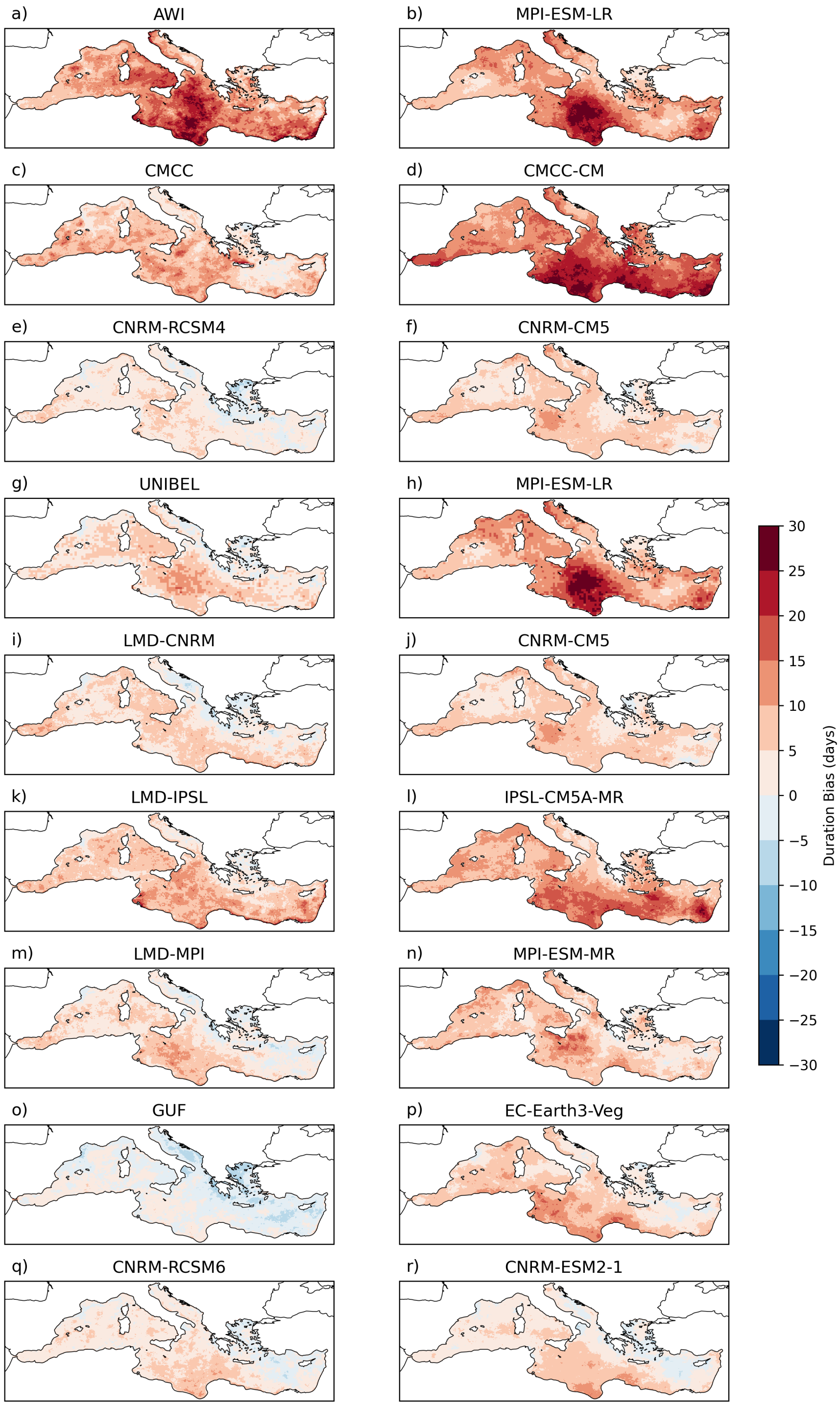

Figure S13. Mean biases in MHW duration for the RCSM (left column) and GCM (right column). MHWs are calculated using a fixed baseline in 1982-2011.

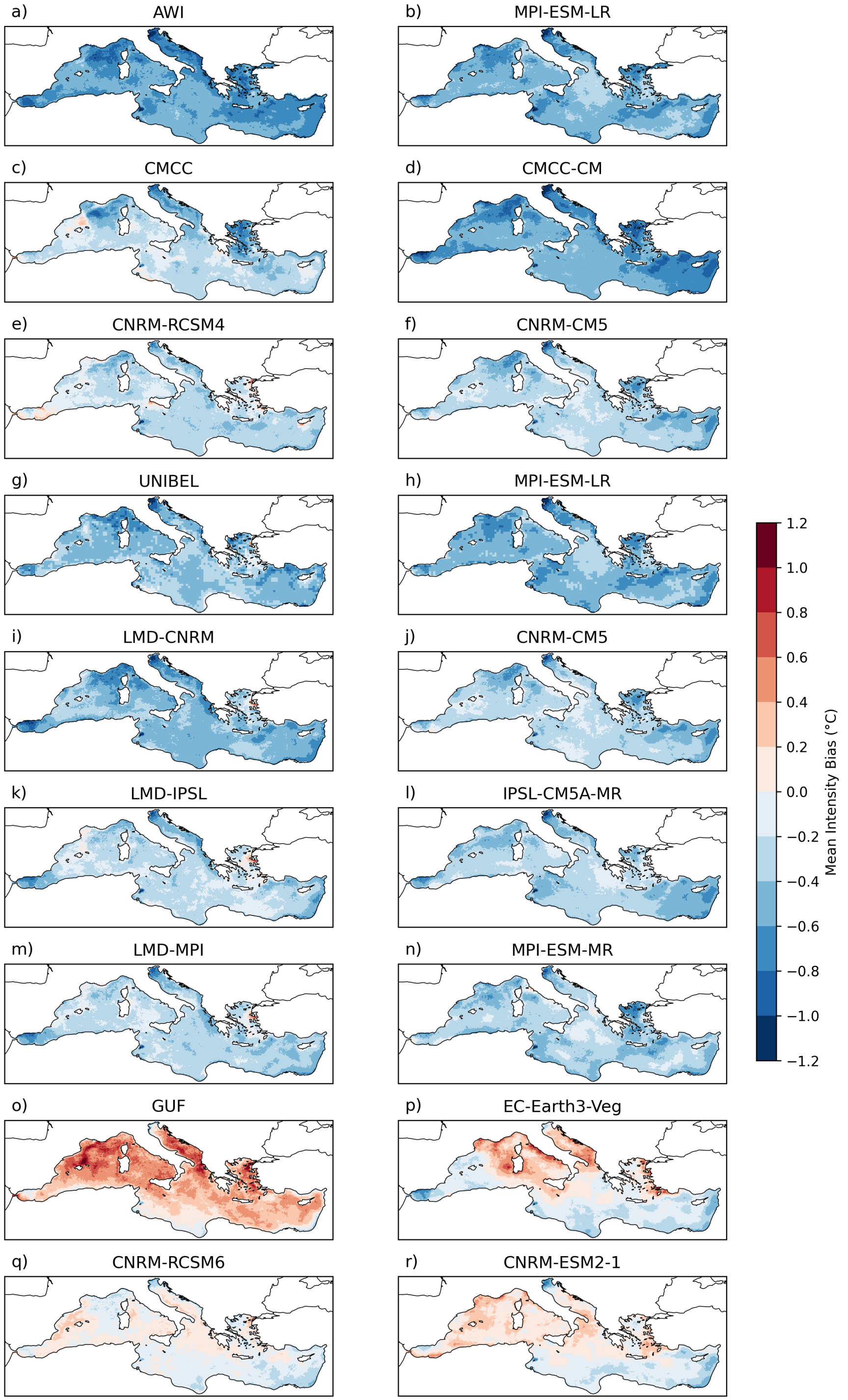

Figure S14. As in Figure S13 but for MHW intensity.

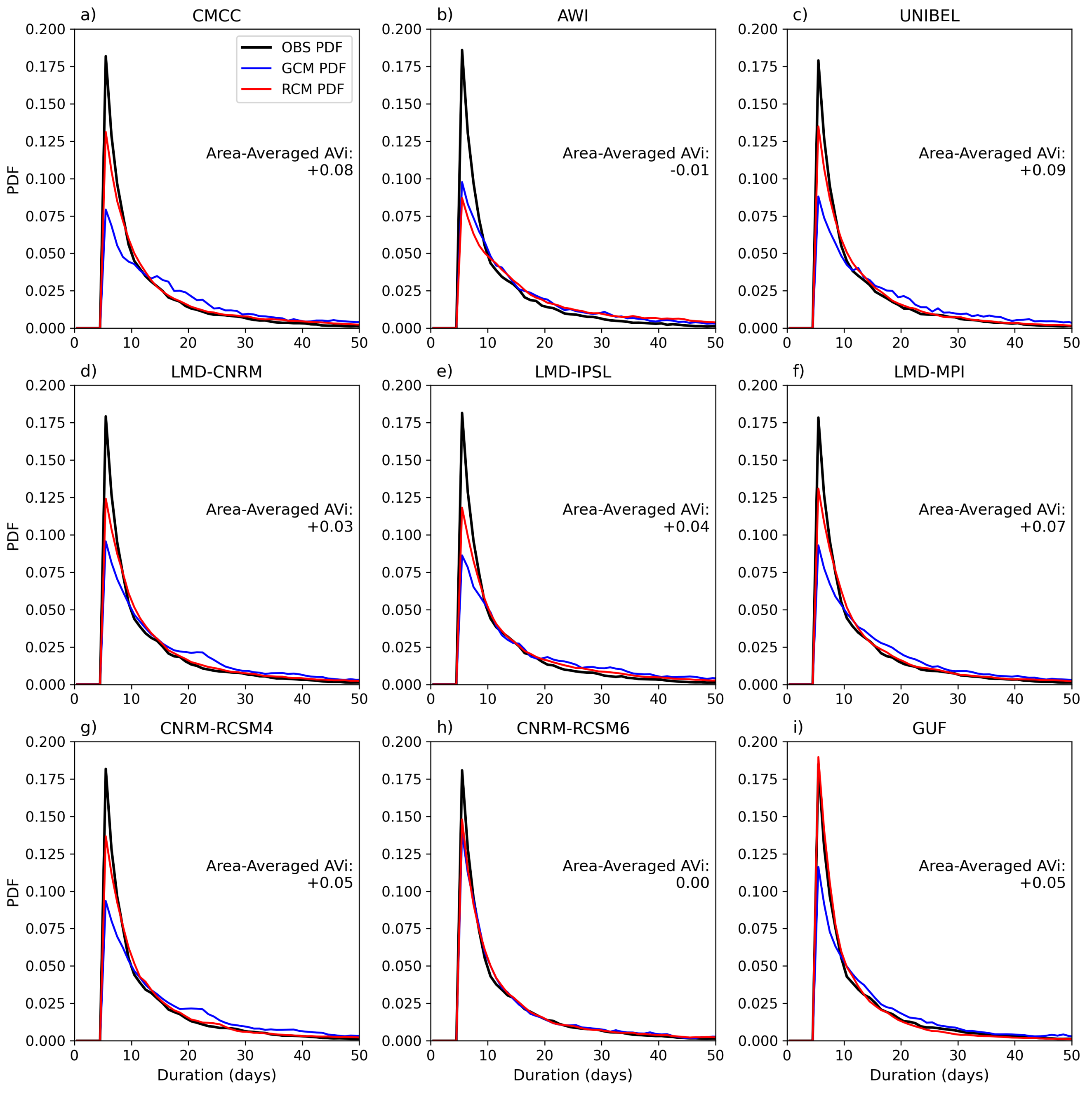

Figure S15. PDFs of aggregated MHW durations over AVi significant grid points for (a) CMCC, (b) AWI, (c) UNIBEL, (d) LMD-CNRM, (e) LMD-IPSL, (f) LMD-MPI, (g) CNRM-RCSM4, (h) CNRM-RCSM6, and (i) GUF. Lines show observations (black), RCSMs (red), and driving GCMs (blue).

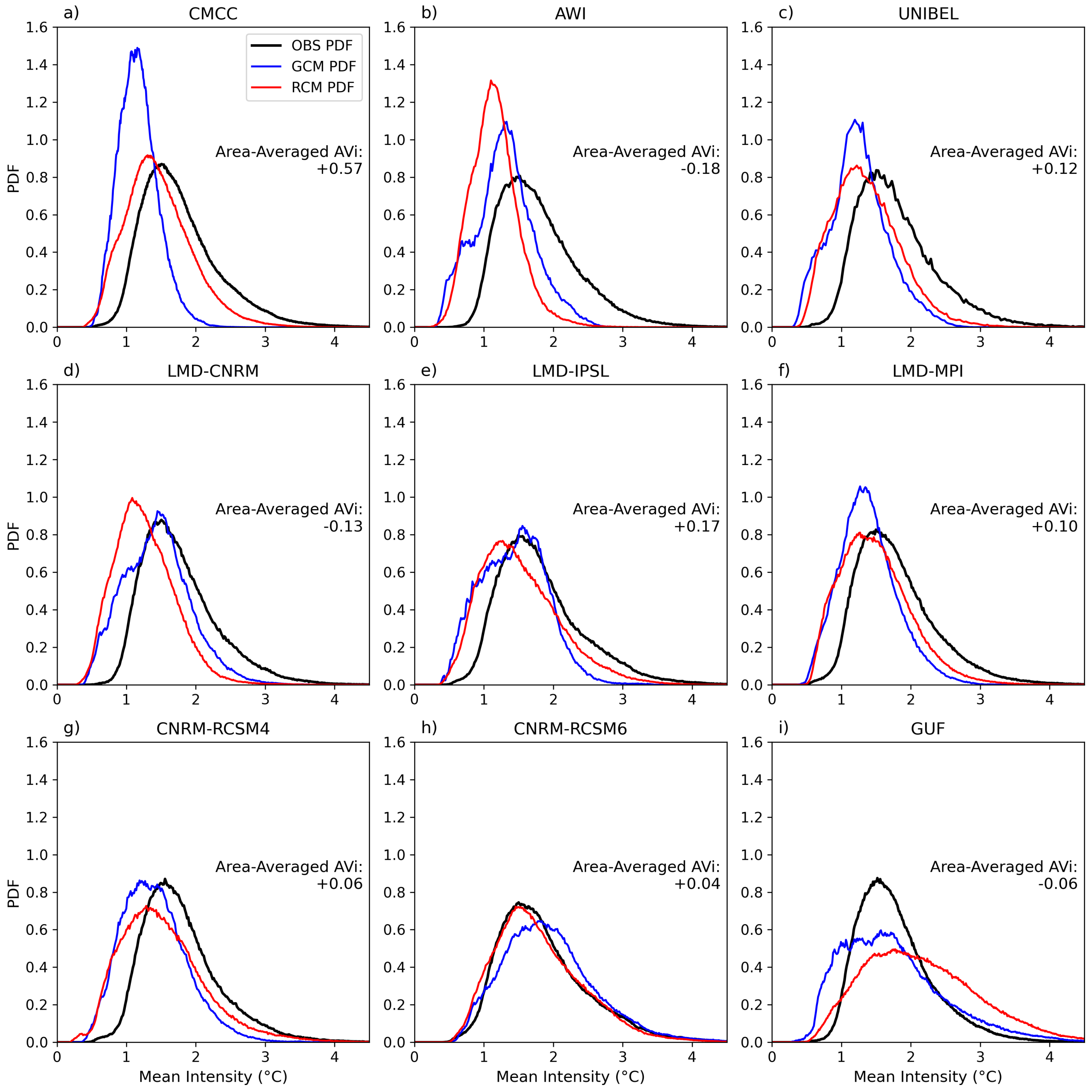

Figure S16. As in Figure S15 but for MHW mean intensity.

References

Buongiorno Nardelli, B., Tronconi, C., Pisano, A., and Santoleri, R.: High and Ultra-High resolution processing of satellite Sea Surface Temperature data over Southern European Seas in the framework of MyOcean project, 129, 1–16, https://doi.org/10.1016/j.rse.2012.10.012, 2013.

Embury, O., Merchant, C. J., Good, S. A., Rayner, N. A., Høyer, J. L., Atkinson, C., Block, T., Alerskans, E., Pearson, K. J., Worsfold, M., McCarroll, N., and Donlon, C.: Satellite-based time-series of sea-surface temperature since 1980 for climate applications, Scientific Data, 11, 326, https://doi.org/10.1038/s41597-024-03147-w, 2024.

Escudier, R., Clementi, E., Cipollone, A., Pistoia, J., Drudi, M., Grandi, A., Lyubartsev, V., Lecci, R., Aydogdu, A., Delrosso, D., Omar, M., Masina, S., Coppini, G., and Pinardi, N.: A High Resolution Reanalysis for the Mediterranean Sea, 9, 702 285, https://doi.org/10.3389/feart.2021.702285, 2021.

Marullo, S., Santoleri, R., Ciani, D., Le Borgne, P., Péré, S., Pinardi, N., Tonani, M., and Nardone, G.: Combining model and geostationary satellite data to reconstruct hourly SST field over the Mediterranean Sea, 146, 11–23, https://doi.org/10.1016/j.rse.2013.11.001, 2014.

Pisano, A., Buongiorno Nardelli, B., Tronconi, C., and Santoleri, R.: The new Mediterranean optimally interpolated pathfinder AVHRR SST Dataset (1982–2012), Remote Sensing of Environment, 176, 107–116, https://doi.org/10.1016/j.rse.2016.01.019, 2016.